Influence of Composition and Process Parameters on Aluminide Coatings Thickness: An Explainable Machine Learning-Assisted Approach

Ali Azari Beni[1], Saeed Rastegari*[1]

[1] School of Metallurgy and Materials Engineering, Iran University of Science and Technology, Narmak, Tehran 1684613114, Iran.

*Corresponding author: Saeed Rastegari, Email: (**Rastegari@iust.ac.ir**)

Abstract

Aluminide coatings are widely used in high-temperature applications due to their excellent corrosion resistance and thermal stability. However, optimizing their composition and thickness is crucial for enhancing performance under varying operational conditions. This study investigates the optimization of aluminide coatings through a data-driven approach, aiming to predict the coating thickness based on various composition and process parameters. A comparative analysis of six machine learning models was conducted, with the k-nearest neighbors regressor (KNNR) demonstrating the highest predictive accuracy, yielding a coefficient of determination R^2 of 0.78, a root mean square error (RMSE) of 18.02 μm, and mean absolute error (MAE) of 14.42. The study incorporates SHAP (Shapley Additive Explanations) analysis to identify the most influential factors in coating thickness prediction. The results indicate that aluminum content (Al), ammonium chloride content (NH_4Cl), and silicon content (Si) significantly impact the coating thickness, with higher Al and Si concentrations leading to thicker coatings. Zirconia (ZrO_2) content was found to decrease thickness due to competitive reactions that hinder Al deposition. Furthermore, the level of activity in the aluminizing process plays a crucial role, with high-activity processes yielding thicker coatings due to faster Al diffusion. The pack cementation method, in particular, produced the thickest coatings, followed by gas-phase and out-of-pack methods. These findings emphasize the importance of optimizing composition and processing conditions to achieve durable, high-performance aluminide coatings for high-temperature applications.

Keywords: Aluminide coatings, Machine learning, Coating thickness prediction, SHAP analysis, Regression models.

1. Introduction

Aluminide coatings, particularly those based on nickel aluminides (β-NiAl), are of significant interest in high-temperature applications due to their exceptional corrosion resistance, creep resistance, and ability to form protective oxide layers [1, 2]. These coatings are typically characterized by the formation of an Al-rich compound on the substrate, resulting in the creation of a stable Al_2O_3 oxide layer at elevated temperatures [3]. The outstanding mechanical properties and high-temperature stability of aluminide coatings make them ideal candidates for use in harsh environments, such as turbine engines and various industrial systems. However, the performance of these coatings is highly dependent on their composition, microstructure, and the precise control of manufacturing processes [4].

Traditional aluminide coating formation methods, such as chemical vapor deposition (CVD) [5-7], pack cementation [8-10], out-of-pack aluminizing [11, 12], and gas-phase aluminizing [13, 14], primarily rely on the diffusion of Al

[DOI: 10.22068/ijmse.4057]

into a substrate, followed by heat treatment to form the desired intermetallic phases. While these techniques have been widely studied, challenges persist in optimizing the composition and thickness of the coatings to improve their performance under various operational conditions.

To further enhance the resistance of aluminide coatings against high-temperature oxidation and hot corrosion induced by sulfide compounds, several modifications have been introduced using Pt [15-17], Si [18, 19], Zr [20-22], Cr [23, 24], and other elements [25, 26]. Si-modified aluminide coatings, created through pack cementation or slurry methods [27], can improve high-temperature oxidation resistance and positively affect resistance to Type II hot corrosion. By forming a diffusion barrier at the coating-substrate interface, they can prevent the infiltration of coating elements into the substrate and enhance the formation of an Al_2O_3 layer. Zr-modified aluminide coatings, which can be produced via pack cementation [28, 29] or sputtering methods [30, 31], improve adhesion at the alumina layer and mitigate the formation of voids at the coating-oxide interface. Zr also inhibits sulfur segregation within these voids and restricts outward Al diffusion during oxidation, resulting in a reduced growth rate of the oxide layer and improved cyclic oxidation behavior [32].

Furthermore, aluminide coatings modified with multiple elements have demonstrated superior properties. For instance, coatings modified with both Pd and Zr exhibit better oxidation resistance compared to those modified with Pd alone [33]. Similarly, Zr and Pt-modified [34] coatings show enhanced oxidation resistance, improved adhesion, and reduced surface roughness when compared to coatings modified with each element separately [35]. Recent advancements in data-driven methodologies, including the use of computational models and machine learning algorithms, offer promising strategies for optimizing these coating processes [36-38]. By leveraging these approaches, it is possible to predict the behavior of aluminide coatings under different conditions, thereby enhancing the efficiency and accuracy of the coating design. These models can account for various factors, such as substrate material, coating thickness, temperature, and heat treatment time, which influence the diffusion behavior and the formation of intermetallic phases like β-NiAl, Ni_2Al_3, and $NiAl_3$ [39].

This paper presents a data-driven approach to predict the thickness of aluminide coatings based on their composition and processing parameters, providing a quantitative framework to guide their optimization. The goal is to develop a predictive model that can guide the design of coatings with superior performance, reducing reliance on experimental trials and accelerating the development of more durable and efficient materials for high-temperature applications.

2. Methodology and model training

The methodology employed in this research is adapted from the approach outlined by Banapour Ghaffari et al. [36, 37, 40, 41]. The dataset used in this study for modeling aluminide coatings was curated from various academic sources, particularly those focused on aluminide coatings applied to superalloys. The data collection process is illustrated in Figure 1, which outlines the steps taken to gather and prepare the dataset. A comprehensive review of the literature was conducted, utilizing key search terms related to aluminide coatings. These terms, used either independently or in combination, included: aluminide coatings, pack cementation, out-of-pack aluminizing, low-activity processes,

[DOI: 10.22068/ijmse.4057]

superalloys, chemical vapor aluminizing, diffusion coatings, nickel aluminides, and both Si-modified and Zr-modified aluminide coatings. The literature search was methodical, ensuring the inclusion of all relevant studies.

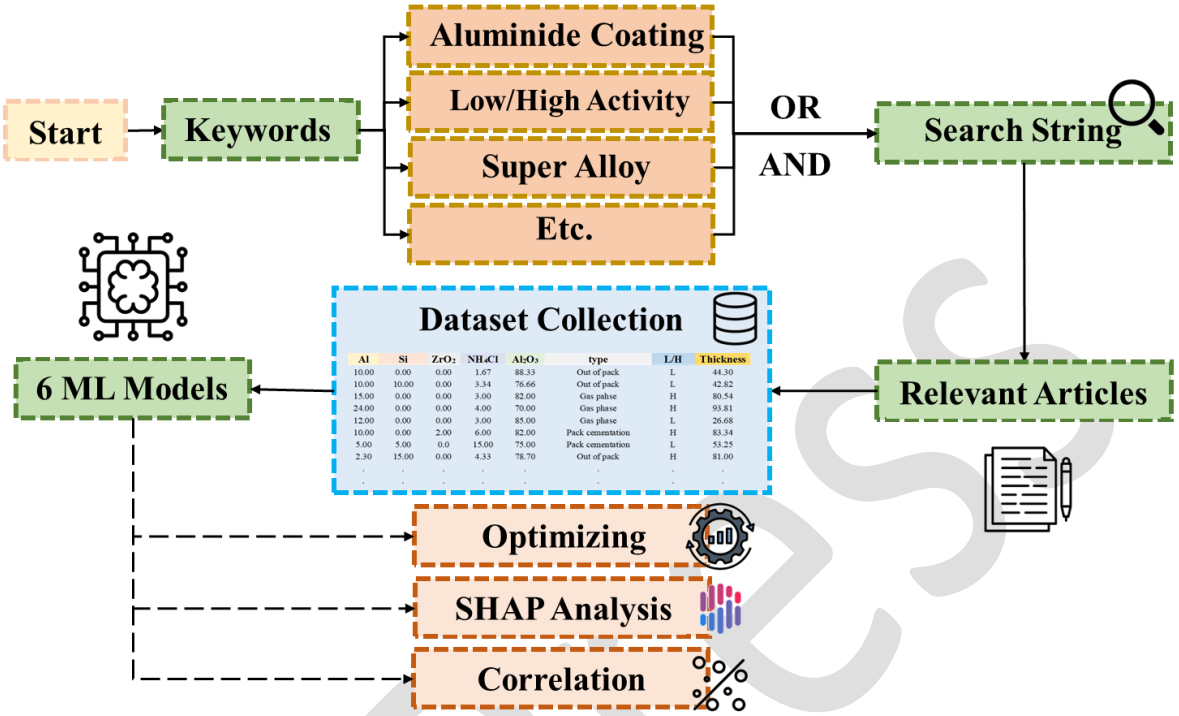

Figure 1. The flowchart of the methodology used in this study.

In Table 1, the input variables, or features, used to predict coating thickness are presented. These variables are critical in developing the prediction model, where the target value is the coating thickness. The selected features include: Al content (wt.%), NH_4Cl content (wt.%), Al_2O_3 content (wt.%), Si content (wt.%), ZrO_2 content (wt.%), the specific coating method (out of pack, pack cementation, or gas-phase aluminizing), and whether the activity level of the Al is low or high. These variables were carefully extracted from the selected academic papers. A series of preprocessing steps were employed to ensure the dataset was in a suitable format for the subsequent model development. Categorical features, specifically 'Coating Method' and 'Activity Level', were converted into a numerical format using one-hot encoding to allow their inclusion in the regression models without implying an ordinal relationship.

During the process of hyperparameter tuning, it is essential to address the presence of outliers—data points that deviate significantly from the general trend of the dataset. These extreme values can distort the model's learning process. Therefore, outliers were identified and removed to improve the reliability of the model. Following the removal of outliers, duplicate entries, if found, were consolidated to further refine the dataset.

Table 1. Description of the variables and inputs of the ML model.

Feature	Description
Al (wt.%)	The percentage of aluminum in the coating.

[DOI: 10.22068/ijmse.4057]

NH_4Cl (wt.%)	The percentage of ammonium chloride used in the coating process.
Al_2O_3 (wt.%)	The percentage of alumina present in the coating.
Si (wt.%)	The percentage of silicon present in the coating.
ZrO_2 (wt.%)	The percentage of zirconia present in the coating.
Coating Method	The method used to apply the aluminide coating (Out of Pack/Pack Cementation/Gas Phase).
Activity Level	The activity level of the Al, either low or high.

This study presents a comparative analysis of six regression models from various families of learning algorithms, aiming to identify the most effective model for predicting coating thickness. The process began with the training and evaluation of a linear regression model [42]. To explore potential non-linear relationships between features and the thickness of the coated layer, five additional regression models were employed: decision tree regressor (DTR) [43], random forest regressor (RFR) [44], k-nearest neighbors regressor (KNNR) [45], support vector machine regressor (SVMR) [46], and multi-layer perceptron regressor (MLPR) [47].

The tree-based models, such as decision trees and random forests, work by partitioning the input space based on feature values and making predictions from the average response within each specific leaf node. On the other hand, the k-nearest neighbors (KNN) regressor operates by predicting values based on the average or weighted average of the target values from the nearest training data points. Support vector machine regression identifies a hyperplane that minimizes the margin between data points, and predictions are made based on the data's position relative to this hyperplane. Neural network regression, which involves interconnected layers learning from input data, predicts outcomes through adjusted weights and biases.

Figure 2 illustrates the process of model selection and training. Initially, the SciPy library [48] was used to conduct descriptive statistics, summarizing the characteristics of the datasets. Hyperparameter values were selected based on these descriptive statistics, and a grid search was conducted to fine-tune the models. Various machine learning regression models from the scikit-learn library [49] were then chosen for tuning and training on each dataset.

Each machine learning model is associated with specific hyperparameters, which must be set before the training process begins. These hyperparameters influence key aspects of the learning process, such as learning rate, iteration count, and model complexity. Unlike model parameters, hyperparameters cannot be learned from the data but play a crucial role in the model's performance and its ability to generalize. As such, identifying the optimal hyperparameter values is essential before training the models. During the training phase, a grid search approach, combined with cross-validation, was used to determine the best hyperparameters for each model, ensuring optimal model performance.

The datasets, having been processed to eliminate inconsistencies or inaccuracies, were randomly split into two sets: the training set and the testing set. This split followed an 80-20 ratio, where 80% of the data was used for training the machine learning models, and the remaining 20% was reserved for testing the model's performance. This 80-20 split is a standard practice in machine learning [37] that provides a large enough dataset for model training while reserving a sufficient, unseen portion for robust performance evaluation. The division of the dataset into training and testing sets was performed randomly, which is a standard practice in machine learning.

[DOI: 10.22068/ijmse.4057]

3. Results and discussion

3.1 Analysis of the collected dataset

Various statistical metrics were employed to assess the numerical data of the datasets, including count, mean, standard deviation, minimum, maximum, and the lower, 50th, and upper percentiles. By default, the lower percentile is set to 25, and the upper percentile to 75. The 25th percentile indicates a value that surpasses a quarter of the data points, while the 50th and 75th percentiles are similarly defined. The 50th percentile, in particular, corresponds to the median. The statistical summary of the datasets is provided in Table 2.

Table 2. The statistical description of the dataset.

	Count	Mean	Standard Deviation	Minimum	25th Percentile	50th Percentile (Median)	75th Percentile	Maximum
Al	103	9.55	7.56	1.8	4	10	10	36
Si	103	3.10	5.38	0	0	0	5	22.5
ZrO_2	103	0.83	1.78	0	0	0	0	9
NH_4Cl	103	4.27	3.56	0	2	4	5	15
Al_2O_3	103	82.25	11.19	41	76.83	85	90	97.5

Figure 2 presents a comprehensive visual summary of the dataset, consisting of multiple subplots that display the distribution of various components. Each subplot represents one variable from the dataset, including the Aluminum content (wt.%) in Figure 2(a), Silicon content (wt.%) in Figure 2(b), ZrO_2 content (wt.%) in Figure 2(c), NH_4Cl content (wt.%) in Figure 2(d), Al_2O_3 content (wt.%) in Figure 2(e), Methods (Out/Gas/Pack) in Figure 2(f), Level of activity in Figure 2(g), and Thickness (μm) in Figure 2(h). The first five subplots (a–e) feature histograms with Kernel Density Estimation (KDE) overlays, providing a clear picture of the distribution of continuous data such as the content of different materials. The (f), (g), and (h) subplots, which present categorical variables, are represented using bar plots. These plots display the frequency of specific categorical values, such as the distribution of methods used (Out of pack, Gas phase, Pack cementation) and the level of activity (Low activity, High activity).

[DOI: 10.22068/ijmse.4057]

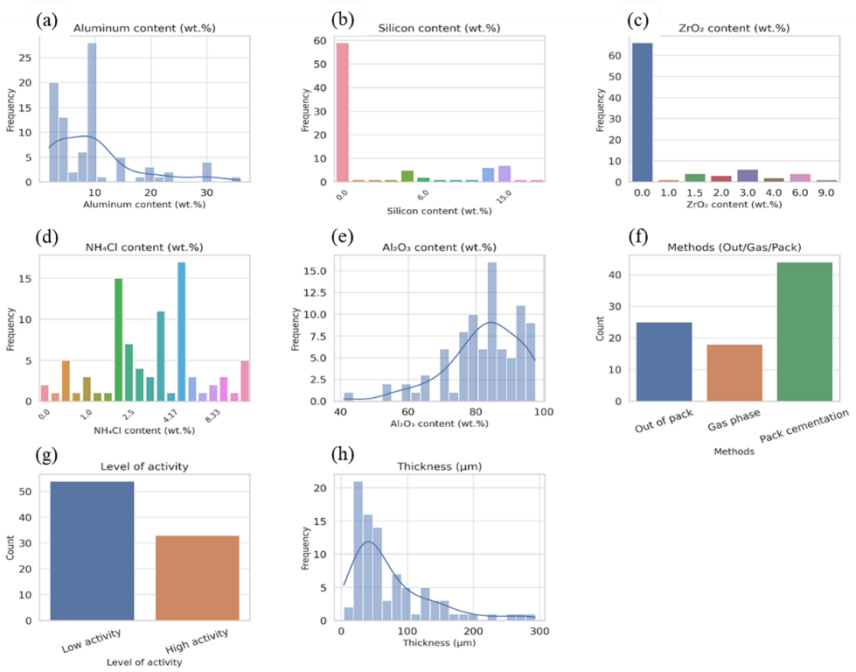

Figure 2. Statistical analysis of the dataset used for model training, showing the distribution of material contents and process parameters: a) Aluminum content (wt.%), b) Silicon content (wt.%), c) ZrO_2 content(wt.%), d) NH_4Cl content (wt.%), e) Al_2O_3 content (wt.%), f) Methods (Out/Gas/Pack), g) Level of activity, h) Thickness (µm).

3.2 Coated thickness prediction model performance

A comparative analysis was performed to identify the most effective machine learning model for predicting the thickness of the coated layer, as detailed in Section 2. The primary objective of this study was to assess the influence of powder composition, process type, and activity level on the accuracy of thickness prediction models. The performance of each model was evaluated using standard metrics commonly applied in regression analysis: the coefficient of determination (R^2), root mean square error (RMSE), and mean absolute error (MAE). The R^2 score, also known as the coefficient of determination, measures the proportion of the variance in the target variable (in this case, coating thickness) that is explained by the independent variables in the model. A higher R^2 value indicates a better fit of the model to the data, with values closer to 1 suggesting that the model explains a large portion of the variability in the predicted outcomes. RMSE quantifies the average magnitude of prediction errors by calculating the square root of the mean squared differences between the predicted and actual values. Complementing this, MAE calculates the average of the absolute differences between predicted and actual values, providing a more direct interpretation of the average error magnitude across all samples.

- $RMSE = \sqrt{\frac{1}{n}\sum_{i=1}^{n}(y_i - \hat{y}_i)^2}$
- $R^2 = 1 - \frac{\sum_{i=1}^{n}(y_i - \hat{y}_i)^2}{\sum_{i=1}^{n}(y_i - \bar{y})^2}$
- $MAE = \frac{1}{n}\sum_{i=1}^{n}|y_i - \hat{y}_i|$

[DOI: 10.22068/ijmse.4057]

In this formula, n represents the number of observations, y_i is the observed value for the i[th] observation, $\hat{y}_i$ is the predicted value for the i[th] observation, and $\bar{y}$ is the mean of the observed values.

Table 3 displays the performance metrics for all models trained in this study. The optimal values for each of the evaluation metrics are highlighted in bold. Overall, the results indicate that non-linear models tend to perform better, confirming the presence of non-linear relationships between the features and the thickness of the coated layer.

Table 3.The performance of various thickness prediction models applied to the dataset.

Model name	R^2	RMSE	MAE
LBR	0.58	28.14	22.51
DTR	0.72	20.35	16.28
RFR	0.61	25.99	20.79
KNNR	**0.78**	**18.02**	**14.42**
SVMR	0.55	27.81	22.25
MLPR	0.69	21.76	17.41

3.3 Explaining the behavior of the thickness prediction model

Figure 3 displays the SHAP (Shapley Additive Explanations) analysis for the features in the thickness prediction model. Each point on the plot represents the SHAP value for a single sample from the dataset, illustrating how that feature impacted the prediction for that specific sample. The points are arranged to show the distribution of SHAP values for each feature. The horizontal axis of the plot corresponds to the SHAP value, which is expressed in the same units as the target property—in this case, the thickness of the coated layer. This value reflects the extent to which each feature influences the predicted thickness.

In the violin plot shown in Figure 3, the feature with the greatest impact, 'Low-activity/High-activity,' is shown at the top of the plot. The features are arranged in descending order of their significance in predicting the thickness. Each data point is colored according to a spectrum on the right side of the plot, which corresponds to the value of the feature. The "feature value" refers to the numerical value of a specific variable in the dataset. For example, the feature "Al (wt.%)" ranges from 1.8 to 36 weight percent (Table 2), with the minimum value (1.8) represented by a blue dot and the maximum (36) by a red dot in the plot. For binary features, such as "level of activity," only two colors—red or blue—are used to indicate either a low or high activity level.

The SHAP analysis presented in Figure 3 identifies the primary factors influencing the prediction of coating thickness as the compositional variables: Al (wt.%), NH_4Cl (wt.%), and Si (wt.%). The results indicate that an increase in the concentrations of these elements corresponds to an increase in the thickness of the coated layer. Conversely, higher concentrations of ZrO_2 (wt.%) lead to a reduction in the coating thickness. Additionally, the activity level of the process plays a significant role in determining the coating thickness, further emphasizing its importance. As shown in

[DOI: 10.22068/ijmse.4057]

Figure 3, Al_2O_3 content has a negligible impact on the predicted thickness, which is consistent with its intended role as a chemically inert filler in the pack mixture.

As shown in Figure 3, high-activity aluminizing results in thicker coatings due to faster Al diffusion at lower temperatures (700–900°C) using aluminum-rich sources. This inward diffusion of Al into the Ni substrate leads to the formation of an Al-rich outer layer (β-NiAl or Ni_2Al_3). The Kirkendall effect generates vacancies, driving compensating outward Ni diffusion and resulting in a thicker coating. In contrast, low-activity aluminizing, which occurs at higher temperatures (950–1100°C) with limited Al supply, results in slower Ni diffusion, forming a thinner coating. High-activity processes sustain a steep concentration gradient that promotes continuous deposition, while low-activity processes use diluted Al sources, leading to limited deposition and thinner coatings [50]. A critical aspect in assessing Al activity lies in its strong dependence on the Al content within the coating powder. Accordingly, Al concentration serves as the primary factor governing both the activity of Al and the resulting thickness of the aluminide coating. However, in the present study, the total Weight of the coating powder was not incorporated into the analysis, which may attenuate the observable influence of Al content on the final coating thickness.

As illustrated in **Error! Reference source not found.**, the thickness of the aluminide coatings increases with higher Si content (wt.%). This phenomenon is attributed to the reactions occurring during the co-deposition process, where Al and Si powders react with NH_4Cl salts to form gaseous species such as AlCl, $SiCl_2$, $SiCl_4$, and SiH_4-yCl_y (y = 1, 2, 3, or 4), as shown in reactions (2), (3),(5), (6), and (7) [51]. At elevated temperatures, only AlCl and $SiCl_2$ species are directly involved in the transfer and deposition of Al and Si onto the substrate, as described in reactions (7) and (8).

$NH_4Cl(g) \rightarrow NH_3(g) + HCl(g)$	[51]	(1)
$2Al(s) + 2HCl(g) \rightarrow 2AlCl(g) + H_2(g)$	[51]	(2)
$Si(s) + 2HCl(g) \leftrightarrow SiCl_2(g) + H_2(g)$	[52]	(3)
$Si(s) + 2HCl(g) \leftrightarrow SiH_2Cl_2(g)$	[52]	(4)
$Si(s) + 3HCl(g) \leftrightarrow SiHCl_3(g) + H_2(g)$	[52]	(5)
$Si(s) + 4HCl(g) \leftrightarrow SiCl_4(g) + 2H_2(g)$	[52]	(6)
$3AlCl(g) \rightarrow 2Al(absorbed) + AlCl_3(g)$	[51]	(7)
$2SiCl_2(g) \rightarrow Si(adsorbed) + SiCl_4(g)$	[52]	(8)

[DOI: 10.22068/ijmse.4057]

The incorporation of Si into aluminide coatings enhances the coating thickness through several interconnected mechanisms, primarily governed by gas-phase transport dynamics. As the Si content in the coating pack increases, additional silicon chloride species—such as $SiCl_2$, SiH_2Cl_2, $SiHCl_2$, and $SiCl_2$—are formed through reactions with HCl, thereby complementing the aluminum chloride transport system. This co-deposition of Si and Al generates a more complex yet favorable environment that promotes thicker coatings [52].

Silicon's presence in the coating matrix significantly influences the diffusion characteristics of aluminum, effectively slowing its inward diffusion while maintaining a high surface Al activity. Moreover, the incorporation of Si alters the phase evolution within the coating, stabilizing certain intermetallic phases. These stabilized phases enable the formation of thicker coatings without the risk of cracking or spallation. Notably, the formation of Si-containing phases, such as Ni-Al-Si ternary compounds, at the coating-substrate interface, results in a more gradual composition gradient. This reduces stress accumulation, thereby facilitating the development of thicker and more durable coatings.
As illustrated in Figure 3, the method of coating is a crucial factor influencing the thickness of aluminide coatings. The order of influence on coating thickness is as follows: 1) pack cementation, 2) gas phase, and 3) out-of-pack cementation. In processes such as pack cementation, a higher Al content in the source powder ensures sustained Al availability, thereby allowing the reaction to proceed for extended durations. This results in deeper Al penetration and a thicker coating. The increased Al content enhances the mobility of Al atoms, facilitating rapid surface migration that contributes to the formation of a uniform oxide layer, which in turn improves high-temperature corrosion resistance.

The increase in Al content within aluminide coatings accelerates the diffusion process and sustains the aluminization reaction, thereby promoting the development of thicker coatings. Simultaneously, higher Al levels enhance chemical activity, which fosters the rapid formation of Al_2O_3 scales, further improving oxidation resistance. However, it is important to avoid excessive Al content, as it can lead to mechanical degradation, as discussed in reaction (9).

$Ni\ (s) + Al\ (diffusing) \rightarrow \beta - NiAl\ (s)$	[51]	(9)

As illustrated in Figure 3, an increase in NH_4Cl content results in an enhanced thickness of aluminide coatings. This is attributed to the decomposition of NH_4Cl, which generates the essential HCl required to convert solid Al into volatile chlorides. An increase in NH_4Cl concentration raises the equilibrium partial pressure of HCl, thereby accelerating the chlorination reactions of Al, Si, and Zr. This, in turn, produces a greater number of Al chloride transport species (e.g., AlCl, $AlCl_2$, $AlCl_3$), significantly enhancing the Al flux to the substrate surface. These gaseous Al chlorides serve as transport agents, delivering Al to the substrate surface, where it reacts with Ni to form the protective β-NiAl intermetallic phase.

The additional HCl produced by the excess NH_4Cl continuously removes surface oxides through the reaction, thereby maintaining active Ni sites for Al incorporation.This process is particularly crucial during the later stages of coating growth, where natural oxide reformation could otherwise hinder further development of the coating [53].

[DOI: 10.22068/ijmse.4057]

It is worth noting that, while higher NH_4Cl concentrations promote thicker coatings, the relationship eventually reaches a point of diminishing returns due to several practical limitations. Excessive NH_4Cl can lead to HCl saturation in the pack atmosphere, where further increases in activator concentration no longer enhance the Al transport rate. Furthermore, the violent gas evolution from NH_4Cl decomposition at elevated concentrations can induce porosity in the coating microstructure. Consequently, modern aluminizing processes carefully optimize NH_4Cl content in relation to other parameters, such as Al particle size, pack composition density, and processing temperature, in order to maximize coating thickness while maintaining the metallurgical integrity of the coating.
The reactions related to aluminide coatings, as shown in reactions (1), (2), and (3). According to these reactions, the amount of Al directly affects the thickness of the coating. Higher Al content increases the chemical potential gradient, accelerating inward diffusion of Al into the substrate.

The thickness of aluminide coatings is directly influenced by the Al content in the deposition process due to fundamental principles of chemical equilibrium and diffusion kinetics. When the Al concentration increases, the system generates more volatile Al chloride species (AlCl, $AlCl_2$, and $AlCl_3$) through reactions with hydrogen chloride (HCl), which is derived from the decomposition of NH_4Cl. These Al chlorides serve as transport agents, carrying Al to the substrate surface where they react with Ni to form the β-NiAl intermetallic phase. Higher Al content shifts the equilibrium of these gas-phase reactions toward greater production of Al chlorides, thereby increasing the flux of Al-bearing species to the substrate. This enhanced transport results in a higher deposition rate of aluminum, which directly contributes to thicker coating formation.

However, while increased Al content promotes coating growth, there are practical limits to this relationship. Excessive Al can lead to undesirable microstructural features, such as Kirkendall porosity, caused by the unequal diffusion rates of Ni and Al. Moreover, if the HCl supply becomes insufficient to chlorinate all available Al, the process transitions from being aluminum-limited to halogen-limited, capping further thickness gains. Therefore, optimizing the aluminum-to-activator ratio is crucial for achieving coatings with the desired thickness and mechanical properties.
The thickness of aluminide coatings decreases with increasing ZrO_2 content due to competitive reactions that divert Al from coating formation and alter the deposition kinetics. The presence of ZrO_2 in the coating powder introduces new reaction pathways that consume aluminum chloride species ($AlCl_3$) to form volatile $ZrCl_4$ through the reaction (10).

$3ZrO_2(s)+4AlCl_3(g) \leftrightarrow 3ZrCl_4(g)+2Al_2O_3(s)$	[54]	(10)

Additionally, the generated $ZrCl_4$ competes with aluminum chloride for deposition sites on the substrate, further limiting Al incorporation into the growing coating as shown in reaction (11).

$ZrCl_4(g)+2AlCl\ (g) \leftrightarrow 2AlCl_3(g)+Zr(absorbed)$	[54]	(11)

[DOI: 10.22068/ijmse.4057]

As ZrO_2 content increases, more Al is diverted to $ZrCl_4$ formation and Zr co-deposition, which disrupts the steady-state Al supply needed for sustained $NiAl$ layer growth [29].

The deposition of Zr also modifies the coating's microstructure and growth mechanism in ways that inherently limit thickness. Unlike Al, which diffuses readily into Ni substrates to form thick intermetallic layers, Zr tends to form localized precipitates or thin surface alloys due to its lower solid-state diffusivity in nickel. This results in a discontinuous growth front that impedes the uniform expansion of the coating. Furthermore, the formation of stable ZrO_2 or Al-Zr-O complexes at the coating-substrate interface acts as diffusion barriers, restricting Al transport into the substrate. While small amounts of Zr can be beneficial, refining the coating's grain structure and improving oxidation resistance, higher concentrations demonstrably limit the achievable thickness.

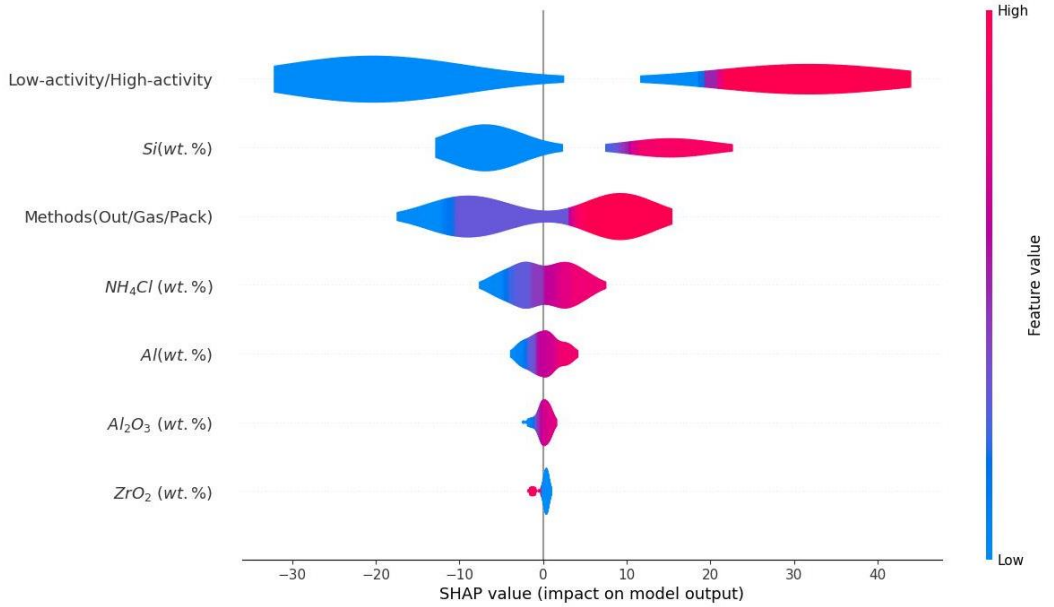

Figure 3. SHAP analysis of the thickness prediction model.

Figure 4 presents the Pearson correlation coefficient for each variable involved in the thickness prediction model. As shown in the figure, the analysis of the Pearson correlation matrix highlights a significant positive relationship between the concentration of Al and the presence of NH_4Cl, underscoring NH_4Cl's function as an activator in the coating deposition process. At elevated temperatures, NH_4Cl undergoes decomposition, yielding HCl gas. This gaseous HCl subsequently reacts with the Al source, typically powdered aluminum, to generate AlCl in the vapor phase. AlCl serves as the primary gaseous precursor for Al, diffusing to the substrate surface (commonly nickel-based alloys) where it reacts to form protective aluminide phases, notably β-NiAl. Consequently, an increased initial quantity of NH_4Cl in the reaction mixture promotes a higher partial pressure of AlCl, leading to enhanced Al diffusion into the substrate and a greater extent of β-NiAl phase formation. The efficiency of this process is highly sensitive to the

[DOI: 10.22068/ijmse.4057]

prevailing temperature and atmospheric conditions within the coating chamber, which directly influence the generation of AlCl and, ultimately, the characteristics of the resultant coating.

Furthermore, a notable positive correlation exists between the activity of Al (represented by the L/H ratio) and the final coating thickness. This observation suggests that the effective Al activity the reactor chamber plays a direct role in determining the deposited layer's thickness. Specifically, positioning the sample in the 'High activity' case, characterized by a higher concentration of gaseous aluminum-bearing species like AlCl, results in an accelerated rate of Al diffusion and thus a thicker coating. Conversely, positioning the sample in the 'Low activity' case, where the concentration of these active species is lower, leads to reduced diffusion rates and thinner coatings. The coating technique employed also exerts a substantial influence on the final thickness of coating. For instance, the Pack Cementation method, where the substrate is embedded in a reactive powder mixture of Al source and activator, ensures a continuous supply of AlCl in close proximity to the sample surface, facilitating sustained diffusion and potentially yielding thicker coatings compared to open-system methods where volatile Al species are continuously swept away. The correlation between the coating method and the L/H ratio is also important, as the Pack technique's tendency to create higher local AlCl concentrations around the sample effectively favors thicker coatings, particularly in the 'High activity' case.

Conversely, the presence of Al_2O_3, often utilized as an inert filler, exhibits a strong negative correlation with Al (-0.72) and NH_4Cl (-0.75), as seen in Figure 4. This is expected, as an increase in the active components necessitates a decrease in the filler material within the powder pack. The primary function of Al_2O_3 is to prevent sintering and moderate reaction kinetics, rather than actively participating in the coating formation, which explains its negligible impact in the SHAP analysis. However, a discernible correlation between Al_2O_3 and the specific coating method employed suggests a potential for physical incorporation of Al_2O_3 particles within the deposited layer, particularly in the pack cementation process, which may be exacerbated if the resulting coatings exhibit a higher degree of porosity. Regarding Si, the absence of a strong correlation with Al indicates that their respective diffusion and reaction pathways are likely independent. While NH_4Cl may facilitate the formation of gaseous precursors for both elements, their subsequent incorporation into the coating layer and the formation of distinct phases appear to be decoupled. This comprehensive analysis underscores the critical importance of carefully controlling activating agent concentrations, the effective Al activity within the reaction environment, and the selection of the appropriate coating methodology to precisely engineer the thickness and composition of protective surface layers.

[DOI: 10.22068/ijmse.4057]

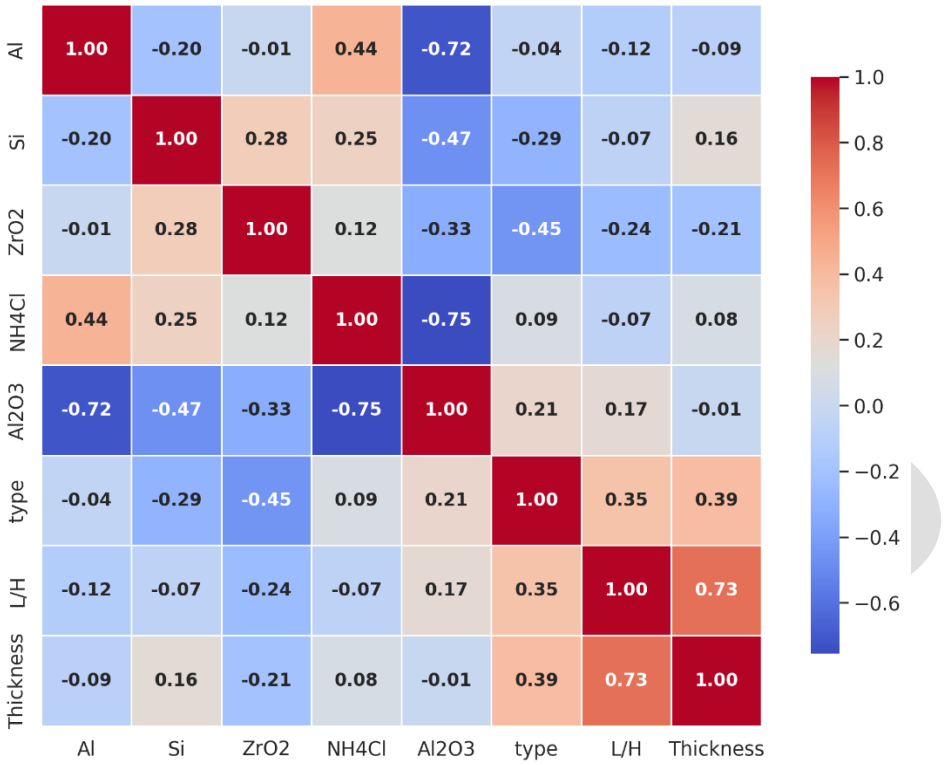

Figure 4. The Pearson correlation coefficient across different variables.

3.4. Limitations and Threats to Validity

While this study offers data-driven insights into the factors influencing aluminide coating thickness, as highlighted by Banapour Ghaffari et al. [36, 37], it is crucial to acknowledge and address the uncertainties inherent in the machine learning models. Adopting their methodology, we must carefully consider these uncertainties to ensure a balanced interpretation. The potential threats to validity can be categorized into external, construct, and internal threats.

The primary threat to external validity (the model's generalizability) is the modest size of the dataset (103 data points). Curating large, consistent datasets is a well-known challenge in materials science. This limitation may contribute to the moderate predictive accuracy (R^2 = 0.55–0.78); therefore, the model should be viewed as a powerful hypothesis-generation tool for guiding experimental work rather than a universally applicable predictive law. Furthermore, data curated from different studies may contain hidden biases from minor, unreported variations in experimental procedures (e.g., furnace ramp rates, powder packing density), which represent a threat to construct validity as they are un-modeled confounding variables.

To mitigate threats to internal validity, such as the inherent randomness in machine learning algorithms, rigorous methodologies were employed. The use of grid search with five-fold cross-validation ensures the reliability of the training procedure, mitigates the risk of overfitting, and identifies the optimal hyperparameters for each model.

Considering these limitations, the causal relationships inferred from the SHAP analysis should be regarded as strong, data-supported hypotheses that require targeted experimental validation. The value of this work lies in its ability to identify the most influential parameters and their effects, providing a clear and quantitative guide for future research.

[DOI: 10.22068/ijmse.4057]

Future work must focus on expanding the dataset and, crucially, validating these data-driven findings with targeted, systematic experiments.

4. Conclusion

This study presents a data-driven approach to optimizing the composition of aluminide coatings by predicting coating thickness using machine learning models. Among the six models tested, the k-nearest neighbors regressor (KNNR) demonstrated the best performance with an R^2 of 0.78, an RMSE of 18.02 µm, and MAE of 14.42, outperforming linear models and thus supporting the non-linear nature of the relationship between coating thickness and the various factors. SHAP analysis revealed that Al content, NH_4Cl content, and Si content were the most influential variables in predicting coating thickness. Specifically, higher Al and Si concentrations directly correlated with increased coating thickness. The activator concentration NH_4Cl was also identified as a critical parameter, as higher levels facilitate the gaseous transport of aluminum required for coating growth. Conversely, ZrO_2 content reduced the thickness due to competing reactions that hindered Al deposition. The activity level of the Al also played a significant role, with high-activity processes leading to thicker coatings due to faster Al diffusion at lower temperatures. Additionally, the pack cementation method produced the thickest coatings, followed by gas-phase and out-of-pack methods. These results provide a clear, data-driven directive for engineering thicker aluminide coatings: processing should utilize high-activity methods like pack cementation, with pack compositions rich in Al and Si, and a carefully optimized activator concentration to maximize deposition kinetics while maintaining microstructural integrity. Future research can focus on increasing the dataset size and diversity, which would likely improve the model's performance and generalization capabilities. Further studies could also examine the impact of other microstructural variables and environmental factors on coating performance, such as temperature cycles, exposure to aggressive environments, and long-term durability.

References

1. Bose, S., Fundamental Concepts. High Temperature Coatings, ed. S. Bose. Butterworth-Heinemann, 2007, 5-16. DOI: https://doi.org/10.1016/B978-075068252-7/50003-2.
2. Agüero, A., Landeira Østergård, M. J., Hansson, A. N. and Gutierrez, M., "Thermal cyclic resistance and long term inter-diffusion properties of slurry aluminide coatings modified with Si." Results in Surfaces and Interfaces., 2022, 6, 100042. DOI: https://doi.org/10.1016/j.rsurfi.2022.100042.
3. Young, D. J., Alloy Oxidation III: Multiphase Scales. High Temperature Oxidation and Corrosion of Metals (Second Edition), ed. D. J. Young. Elsevier, 2016, 335-392. DOI: https://doi.org/10.1016/B978-0-08-100101-1.00007-8.
4. Mojaddami, M., Rastegari, S., Arabi, H. and Rafiee, H., "Effect of heat treatment on coating microstructure applied by high activity diffusion process on IN738LC." Surface engineering., 2012, 28, 772-777. DOI: 10.1179/1743294412Y.0000000064.

[DOI: 10.22068/ijmse.4057]

5. Angenete, J. and Stiller, K., "Comparison of inward and outward grown Pt modified aluminide diffusion coatings on a Ni based single crystal superalloy." Surface and coatings Technology., 2002, 150, 107-118. DOI: https://doi.org/10.1016/S0257-8972(01)01544-4.
6. Shao, M., Mo, W., Wu, Y., Sun, Q., Xia, S., Wang, Y., Fang, H. and Nishimura, K., "Research on the microstructure and diffusion behavior of CVD aluminide coatings on inconel 718 superalloy." Vacuum., 2024, 228, 113541. DOI: https://doi.org/10.1016/j.vacuum.2024.113541.
7. Xu, J., Geng, S., Wang, J., Chen, G., Wang, F., Sun, Q., Xia, S. and Wu, Y., "Effect of deposition temperature on corrosion behavior of CVD aluminide coatings on K452 superalloy." Surface and Coatings Technology., 2025, 496, 131600. DOI: https://doi.org/10.1016/j.surfcoat.2024.131600
8. Wu, Y., Zhang, Z., Leng, J., Gao, C., Huang, G., Qi, F., Lu, T. and Shi, Q., "Supercritical oxidation resistance of double-layer aluminized coating on Nickel alloy prepared by pack cementation aluminizing." Surface and Coatings Technology., 2025, 497, 131728. DOI: https://doi.org/10.1016/j.surfcoat.2025.131728.
9. Yener, T., Erdogan, A., Doleker, K. M., Nalburoğlu, G. and Efe, G. C., "Protective nickel silicide coating on Inconel 738 superalloy: Microstructure and wear behavior." Materials Today Communications., 2025, 43, 111643. .DOI: https://doi.org/10.1016/j.mtcomm.2025.111643.
10. Pauletti, E. and d'Oliveira, A. S. C. M., "Study on the mechanisms of formation of aluminized diffusion coatings on a Ni-base superalloy using different pack aluminization procedures." Journal of Vacuum Science & Technology A., 2018, 36, 041504. DOI: 10.1116/1.5026272.
11. Rezaee, B., Rastegari, S. and Eyvazjamadi, H., "Formation mechanism of Pt-modified aluminide coating structure by out-of-the-pack aluminizing." Surface Engineering., 2021, 37, 343-350. .DOI: 10.1080/02670844.2020.1741212.
12. Goral, M., Ochal, K., Kubaszek, T. and Drajewicz, M., "The influence of deposition technique of aluminide coatings on oxidation resistance of different nickel superalloys." Materials Today: Proceedings., 2020, 33, 1746-1751. DOI: https://doi.org/10.1016/j.matpr.2020.04.863
13. Lin, H. J., Sun, W. P. and Hon, M. H., "Gas phase aluminide coatings on nickel-base superalloy in 713." Thin Solid Films., 1988, 156, 259-264. DOI: https://doi.org/10.1016/0040-6090(88)90319-7.
14. Rafiee, H., Arabi, H. and Rastegari, S., "Effects of temperature and Al-concentration on formation mechanism of an aluminide coating applied on superalloy IN738LC through a single step low activity gas diffusion process." Journal of alloys and compounds., 2010, 505, 206-212. DOI: https://doi.org/10.1016/j.jallcom.2010.06.030.
15. Swadźba, R., Hetmańczyk, M., Sozańska, M., Witala, B. and Swadźba, L., "Structure and cyclic oxidation resistance of Pt, Pt/Pd-modified and simple aluminide coatings on CMSX-4 superalloy." Surface and Coatings Technology., 2011, 206, 1538-1544. DOI: https://doi.org/10.1016/j.surfcoat.2011.06.042.
16. Reed, R. C., Wu, R. T., Hook, M. S., Rae, C. M. F. and Wing, R. G., "On oxidation behaviour of platinum aluminide coated nickel based superalloy CMSX-4." Materials Science and Technology., 2009, 25, 276-286. DOI: 10.1179/174328408X361481.

[DOI: 10.22068/ijmse.4057]

17. Pauletti, E. and d'Oliveira, A. S. C. M., "Influence of Pt concentration on structure of aluminized coatings on a Ni base superalloy." Surface and Coatings Technology., 2017, 332, 57-63. DOI: https://doi.org/10.1016/j.surfcoat.2017.10.052.
18. Wang, W., Li, Z., Lei, Y., Wu, M., Cheng, Y., Shen, M., Zhu, S. and Wang, F., "Si modified aluminide coatings on a Ni-base superalloy prepared using Al-Si plasma irradiation: Growth mechanism and oxidation behavior." Surface and Coatings Technology., 2024, 494, 131425. DOI: https://doi.org/10.1016/j.surfcoat.2024.131425.
19. He, H., Liu, Z., Wang, W. and Zhou, C., "Microstructure and hot corrosion behavior of Co–Si modified aluminide coating on nickel based superalloys." Corrosion Science., 2015, 100, 466-473. DOI: https://doi.org/10.1016/j.corsci.2015.08.011.
20. Khakpour, I., Soltani, R. and Sohi, M. H., "Microstructure and High Temperature Oxidation Behaviour of Zr-Doped Aluminide Coatings Fabricated on Nickel-based Super Alloy." Procedia Materials Science., 2015, 11, 515-521. DOI: https://doi.org/10.1016/j.mspro.2015.11.011.
21. Zagula-Yavorska, M., Pytel, M., Romanowska, J. and Sieniawski, J., "The Effect of Zirconium Addition on the Oxidation Resistance of Aluminide Coatings." Journal of Materials Engineering and Performance., 2015, 24, 1614-1625. DOI: 10.1007/s11665-015-1421-5
22. Latifi, R., Rastegari, S. and Razavi, S. H., "Effect of ZR Content on Oxide-Scale Spallation of Aluminide Coating." Iran. J. Mater. Sci. Eng., 2019, 16, 63. DOI: 10.22068/ijmse.16.4.63.
23. Wu, D., Jiang, S., Fan, Q., Gong, J. and Sun, C., "Hot Corrosion Behavior of a Cr-Modified Aluminide Coating on a Ni-Based Superalloy." Acta Metallurgica Sinica (English Letters)., 2014, 27, 627-634. DOI: 10.1007/s40195-014-0108-5.
24. Le Guével, Y., Grégoire, B., Cristóbal, M. J., Feaugas, X., Oudriss, A. and Pedraza, F., "Dissolution and passivation of aluminide coatings on model and Ni-based superalloy." Surface and Coatings Technology., 2019, 357, 1037-1047. DOI: https://doi.org/10.1016/j.surfcoat.2018.10.090.
25. Safari, M. and Nogorani, F. S., "Formation mechanism of high activity aluminide coating on Ni-CeO_2 coated Rene 80 alloy." Surface and Coatings Technology., 2017, 329, 218-223. DOI: https://doi.org/10.1016/j.surfcoat.2017.09.035.
26. Tolpygo, V. K., Murphy, K. S. and Clarke, D. R., "Effect of Hf, Y and C in the underlying superalloy on the rumpling of diffusion aluminide coatings." Acta Materialia., 2008, 56, 489-499. DOI: https://doi.org/10.1016/j.actamat.2007.10.006.
27. Bakhtiary, O., Sarraf, S. and Soltanieh, M., "Microstructure evaluation of Si-modified aluminide coatings on IN625 deposited by slurry aluminizing process." Surface and Coatings Technology., 2025, 495, 131592. DOI: https://doi.org/10.1016/j.surfcoat.2024.131592.
28. Zhou, Y., Zhao, X., Zhao, C., Hao, W., Wang, X. and Xiao, P., "The oxidation performance for Zr-doped nickel aluminide coating by composite electrodepositing and pack cementation." Corrosion Science., 2017, 123, 103-115. DOI: https://doi.org/10.1016/j.corsci.2017.04.008.

[DOI: 10.22068/ijmse.4057]

29. Zare Mohazabie, M. S. and Nogorani, F. S., "The addition of zirconium to aluminide coatings: The effect of the aluminide growth mode." Surface and Coatings Technology., 2019, 378, 125066. DOI: https://doi.org/10.1016/j.surfcoat.2019.125066.
30. Tiwari, S. K., Rao, A. U., Kharb, A. S., Verma, P. C., Dubey, P., Chawla, V., Sardana, N., Kumar, S., Avasthi, D. K. and Chawla, A. K., "Sputter-deposited zirconium doped nickel-aluminide coatings for high-temperature oxidation-resistant applications." Journal of Vacuum Science & Technology A., 2024, 42, 053408. DOI: 10.1116/6.0003848.
31. Hamadi, S., Bacos, M. P., Poulain, M., Seyeux, A., Maurice, V. and Marcus, P., "Oxidation resistance of a Zr-doped NiAl coating thermochemically deposited on a nickel-based superalloy." Surface and Coatings Technology., 2009, 204, 756-760. DOI: https://doi.org/10.1016/j.surfcoat.2009.09.073.
32. Zagula-Yavorska, M., Sieniawski, J. and Romanowska, J., "Oxidation behaviour of zirconium-doped NiAl coatings deposited on pure nickel." Archive of Materials Science and Engineering., 2012, 58, 250-254.
33. Romanowska, J., Morgiel, J. and Zagula-Yavorska, M., "The Influence of Pd and Zr Co-Doping on the Microstructure and Oxidation Resistance of Aluminide Coatings on the CMSX-4 Nickel Superalloy." Materials., 2021, 14, 7579. DOI: 10.3390/ma14247579.
34. Hong, S. J., Hwang, G. H., Han, W. K., Lee, K. S. and Kang, S. G., "Effect of zirconium addition on cyclic oxidation behavior of platinum-modified aluminide coating on nickel-based superalloy." Intermetallics, 2010, 18, 864-870. DOI: https://doi.org/10.1016/j.intermet.2008.08.014.
35. Hong, S. J., Hwang, G. H., Han, W. K. and Kang, S. G., "Cyclic oxidation of Pt/Pd-modified aluminide coating on a nickel-based superalloy at 1150°C." Intermetallics., 2009, 17, 381-386. DOI: https://doi.org/10.1016/j.intermet.2008.08.014.
36. Banapour Ghaffari, O., Eftekhari Yekta, B. and Zakeri-Nasrabadi, M., "Estimating "depth of layer" (DOL) in ion-exchanged glasses using explainable machine learning." Materialia., 2024, 33, 102027. DOI: https://doi.org/10.1016/j.mtla.2024.102027.
37. Banapour Ghaffari, O., Eftekhari Yekta, B. and Zakeri-Nasrabadi, M., "Designing high-performance ion-exchangeable glasses with multi-objective optimization and machine learning." Ceramics International., 2024, 50, 42949-42962. DOI: https://doi.org/10.1016/j.ceramint.2024.08.141.
38. Juez Lorenzo, M. M., Kolarik, V., Sethia, K. and Strakos, P., "Segmentation and Metallographic Evaluation of Aluminium Slurry Coatings Using Machine Learning Techniques." High Temperature Corrosion of Materials., 2024, 101, 1497-1512. DOI: 10.1007/s11085-024-10321-3.
39. Brossard, J. M., Panicaud, B., Balmain, J. and Bonnet, G., "Modelling of aluminized coating growth on nickel." Acta Materialia., 2007, 55, 6586-6595. DOI: https://doi.org/10.1016/j.actamat.2007.08.025.
40. Banapour Ghaffari, O., Fadaei, A., Lotfipoor, P. and Eftekhari Yekta, B., "Strengthening of soda-lime glasses using field-assisted ion exchange." Journal Of Metallurgical and Materials Engineering., 2024, 35, 1-16. DOI: https://doi.org/10.22067/jmme.2024.84990.1127.
41. Eftekhari Yekta, B. and Banapour Ghafari, O., "Electrical Conductivity in the Molten and Glassy States of the $Li_2(O, Cl_2, I_2)$-B_2O_3 system." Iran. J. Mater. Sci. Eng., 2023, 20, 1. DOI: 10.22068/ijmse.3300.

[DOI: 10.22068/ijmse.4057]

42. Fraza, C. J., Dinga, R., Beckmann, C. F. and Marquand, A. F., "Warped Bayesian linear regression for normative modelling of big data." NeuroImage., 2021, 245, 118715. DOI: https://doi.org/10.1016/j.neuroimage.2021.118715.
43. Quinlan, J. R., "Induction of decision trees." Machine Learning., 1986, 1, 81-106.
44. Breiman, L., "Random Forests." Machine Learning., 2001, 45, 5-32. DOI: 10.1023/A:1010933404324.
45. Cover, T. and Hart, P., "Nearest neighbor pattern classification." IEEE Transactions on Information Theory., 1967, 13, 21-27.
46. Cortes, C. and Vapnik, V., "Support-vector networks." Machine Learning., 1995, 20, 273-297. DOI: 10.1007/BF00994018.
47. Rosenblatt, F., "The perceptron: A probabilistic model for information storage and organization in the brain." Psychological Review., 1958, 65, 386-408. DOI: 10.1037/h0042519.
48. Virtanen, P., Gommers, R., Oliphant, T. E., Haberland, M., Reddy, T., Cournapeau, D., Burovski, E., Peterson, P., Weckesser, W., Bright, J., van der Walt, S. J., Brett, M., Wilson, J., Millman, K. J., Mayorov, N., Nelson, A. R. J., Jones, E., Kern, R., Larson, E., Carey, C. J., Polat, İ., Feng, Y., Moore, E. W., VanderPlas, J., Laxalde, D., Perktold, J., Cimrman, R., Henriksen, I., Quintero, E. A., Harris, C. R., Archibald, A. M., Ribeiro, A. H., Pedregosa, F., van Mulbregt, P., Vijaykumar, A., Bardelli, A. P., Rothberg, A., Hilboll, A., Kloeckner, A., Scopatz, A., Lee, A., Rokem, A., Woods, C. N., Fulton, C., Masson, C., Häggström, C., Fitzgerald, C., Nicholson, D. A., Hagen, D. R., Pasechnik, D. V., Olivetti, E., Martin, E., Wieser, E., Silva, F., Lenders, F., Wilhelm, F., Young, G., Price, G. A., Ingold, G.-L., Allen, G. E., Lee, G. R., Audren, H., Probst, I., Dietrich, J. P., Silterra, J., Webber, J. T., Slavič, J., Nothman, J., Buchner, J., Kulick, J., Schönberger, J. L., de Miranda Cardoso, J. V., Reimer, J., Harrington, J., Rodríguez, J. L. C., Nunez-Iglesias, J., Kuczynski, J., Tritz, K., Thoma, M., Newville, M., Kümmerer, M., Bolingbroke, M., Tartre, M., Pak, M., Smith, N. J., Nowaczyk, N., Shebanov, N., Pavlyk, O., Brodtkorb, P. A., Lee, P., McGibbon, R. T., Feldbauer, R., Lewis, S., Tygier, S., Sievert, S., Vigna, S., Peterson, S., More, S., Pudlik, T., Oshima, T., Pingel, T. J., Robitaille, T. P., Spura, T., Jones, T. R., Cera, T., Leslie, T., Zito, T., Krauss, T., Upadhyay, U., Halchenko, Y. O., Vázquez-Baeza, Y. and SciPy, C., "SciPy 1.0: fundamental algorithms for scientific computing in Python." Nature Methods., 2020, 17, 261-272. DOI: 10.1038/s41592-019-0686-2.
49. Pedregosa, F., Varoquaux, G., Gramfort, A., Michel, V., Thirion, B., Grisel, O., Blondel, M., Prettenhofer, P., Weiss, R. and Dubourg, V., "Scikit-learn: Machine learning in Python." the Journal of machine Learning research., 2011, 12, 2825-2830.
50. Bianco, R. and Rapp, R. A., "Pack cementation diffusion coatings." Metallurgical and ceramic protective coatings., 1996, 236-260.
51. Azari Beni, A. and Rastegari, S., "Microstructural investigation of low-activity and high-activity aluminide coatings fabricated by vapor phase aluminizing on IN792 superalloy." Scientific Reports., 2025, 15, 25284. DOI: https://doi.org/10.1038/s41598-025-10549-2.

[DOI: 10.22068/ijmse.4057]

52. Fu, C., Kong, W. and Cao, G., “Microstructure and oxidation behavior of Al+ Si co-deposited coatings on nickel-based superalloys.” Surface and Coatings Technology., 2014, 258, 347-352. DOI: https://doi.org/10.1016/j.surfcoat.2014.09.003.
53. Eslami, A., Arabi, H. and Rastegari, S., “Gas Phase Aluminizing of a Nickel Base Superalloy by a Single Step HTHA Aluminizing Process.” Canadian Metallurgical Quarterly., 2009, 48, 91-98. DOI: 10.1179/cmq.2009.48.1.91.
54. Mohazabie, M. Z. and Nogorani, F. S., “The addition of zirconium to aluminide coatings: The effect of the aluminide growth mode.” Surface and Coatings Technology., 2019, 378, 125066.

[DOI: 10.22068/ijmse.4057]